Available online at www.sciencedirect.com
SCIENCE DIRECT®
Journal of Crystal Growth 267 (2004) 703–713
JOURNAL OF CRYSTAL GROWTH
www.elsevier.com/locate/jcrysgro

Nonlinear theory of self-similar crystal growth and melting

Shuwang Li[a,b], John S. Lowengrub[b,c,*], Perry H. Leo[a], Vittorio Cristini[b,d]

[a] *Department of Aerospace Engineering and Mechanics, University of Minnesota, Minneapolis, MN 55455, USA*
[b] *Department of Mathematics, University of California at Irvine, 103 MSTB, Irvine, CA 92612, USA*
[c] *School of Mathematics, University of Minnesota, Minneapolis, MN 55455, USA*
[d] *Department of Biomedical Engineering, University of California at Irvine, Irvine, CA 92612, USA*

Received 20 January 2004; accepted 2 April 2004

Communicated by G.B. McFadden

Abstract

In this paper, we demonstrate the existence of noncircular shape-invariant (self-similar) growing and melting two-dimensional crystals. This work is motivated by the recent three-dimensional studies of Cristini and Lowengrub in which the existence of self-similar shapes was suggested using linear analysis (J. Crystal Growth, 240 (2002) 267) and dynamical numerical simulations (J. Crystal Growth 240 (2003) in press). Here, we develop a nonlinear theory of self-similar crystal growth and melting. Because the analysis is qualitatively independent of the number of dimensions, we focus on a perturbed two-dimensional circular crystal growing or melting in a liquid ambient. Using a spectrally accurate quasi-Newton method, we demonstrate that there exist nonlinear self-similar shapes with k-fold dominated symmetries. A critical heat flux J_k is associated with each shape. In the isotropic case, k is arbitrary and only growing solutions exist. When the surface tension is anisotropic, k is determined by the form of the anisotropy and both growing and melting solutions exist. We discuss how these results can be used to control crystal morphologies during growth.

PACS: 81.10.A; 64.70.D

Keywords: A1. Diffusion; A1. Morphological stability; A1. Mullins–Sekerka instability; A1. Quasi–Newton method; A2. Compact growth; A2. Self-similar

1. Introduction

Crystal growth is a classical example of a phase transformation from the liquid phase to the solid phase via heat transfer. A well-known and remarkable feature observed during the phase transformation is the occurrence of various patterns and morphologies of the solid/liquid interface–flat, cellular or dendritic. The patterns depend on the initial conditions, the composition of the liquid phase, the interfacial crystallographic properties, the supercooling and the applied far-field flux. Because of its importance, these phase transforma-

*Corresponding author. Department of Mathematics, University of California at Irvine, Irvine, CA 92612, USA. Tel.: +9498242655; fax: +9498247993.
E-mail addresses: sli@aem.umn.edu (S. Li), lowengrb@math.uci.edu (J. S. Lowengrub).

0022-0248/$ - see front matter
doi:10.1016/j.jcrysgro.2004.04.002

tions have received considerable attention from the materials research community, see Refs. [3–7]. Much of this research is concerned with detailed and extensive studies of dendritic growing shapes. We note that in very recent work, Glicksman et al. [8] developed a quasi-static theory to describe self-similar melting of prolate spheroids in the absence of surface tension. Good agreement between this theory and data of melting dendrite fragments in microgravity was attained although surface tension effects were observed near the dissolution time [8]. Here, we focus our study on the growth and melting of compact self-similar crystals in a pure liquid phase without any restrictions on the crystal morphology and in the presence of both isotropic and anisotropic surface tension.

Historically, studies of the growth and equilibrium shapes of crystals arise from the desire to understand and control material production. This has led to many interesting and fundamental problems involving the geometry of surfaces. For example, Wulff first developed the concept that the equilibrium shape is given by minimizing the total surface free energy of a crystal at a fixed volume [9]. For a two dimensional crystal with fixed area, for instance, the equilibrium shape is a circle if the surface energy is isotropic.

The morphology of a growing crystal is complicated by the dynamics of diffusing heat through the system. A number of models have been used to describe the morphology during crystal growth, see Refs. [7,10–12] among many others. Using a quasi-steady model, Mullins and Sekerka were the first to perform a linear morphological stability analysis of growing crystals in a supercooled liquid [13]. They investigated the behavior of an infinitesimal perturbation of a spherical solid by a single spherical harmonic, and found that below a critical radius the perturbation decays and above the critical radius the perturbation grows. The critical radius depends on the polar perturbation wavenumber and on the supercooling. As the crystal grows, larger and larger wavenumbers become unstable, leading to the development of complex shapes (e.g. snowflakes) [13,17]. Mullins and Sekerka [13] also identified the possibility of growing crystals with compact shapes when the supercooling is kept sub-critical by interparticle interactions. This was not quantified further, however. Coriell and Parker performed an analogous linear analysis for a growing cylinder [14,18]. Hardy and Coriell conducted an experiment of a single crystal ice cylinder and found that the growth rates of perturbations in the circular shape of the cylinder are in agreement with the predictions of the linear stability analysis [15,16].

Recently, Cristini and Lowengrub [1,2] reconsidered the three-dimensional quasi-steady crystal growth problem studied originally by Mullins–Sekerka[13] and Coriell–Parker[14,18], and suggested that there exist critical conditions of an imposed far-field heat flux (rather than a far-field supercooling) such that the classical Mullins–Sekerka instability can be suppressed and that the morphologies of growing crystals can be compact and controlled. This quantifies and goes beyond the prediction of Mullins and Sekerka [13]. Using linear analysis Cristini and Lowengrub [1] also found that there exist critical conditions of flux for which the growth of nonspherical crystals is actually self-similar. Note that what we mean by flux in Refs. [1,2] and this paper is the integral flux applied at the far-field boundary. Using a 3D adaptive boundary integral method, Cristini and Lowengrub [2] performed dynamical simulations that suggest the existence of nonlinear self-similar shapes.

For an isolated quasi-steady evolving crystal, an imposed far-field heat flux J represents the rate of area (2D) or volume (3D) change in time. The heat flux and the supercooling ΔT are related by $J \sim -R\Delta T$, in 3D [19,2] and by $J \sim -\log(1/R)\Delta T$ in 2D where R is the effective radius of the crystal (radius of a sphere with the same volume) and ΔT denotes the difference between the far-field temperature and the phase change temperature for a flat interface[19,2]. Thus, conditions of specified flux can be enforced by varying ΔT with the crystal radius.

In this paper, we extend the recent studies of Cristini and Lowengrub [1,2] by developing a nonlinear theory of self-similar crystal growth. We focus on 2D crystals. Our analysis reveals that the governing equations for nonlinear self-similar crystals are qualitatively similar in 2D and 3D once the difference between the 2D and 3D heat fluxes (i.e. area vs. volume growth) is scaled out.

Therefore our work here provides insight to the 3D nonlinear problem.

We focus our study on a perturbed circular crystal growing in an supercooled liquid. We derive the governing equations for nonlinear self-similar growth, and implement a quasi-Newton method to solve these equations numerically. The equation takes the form of a highly nonlinear, nonlocal eigenvalue problem where the shape is the eigenvector and the heat flux is the eigenvalue. Our numerical results indicate that nonlinear, noncircular self-similarly evolving crystals do indeed exist. From the solution to these equations, we obtain the self-similar shape and the associated nonlinear critical far-field heat flux. Our numerical results reveal that for a k-fold dominant self-similar shape (with k arbitrary), only mode k and its harmonics (integer multiples of the wavenumber k) appear in the Fourier series description of the interface.

One of the effects of nonlinearity is to reduce the nonlinear critical flux compared to that predicted by linear theory. One of the effects of anisotropy is to reduce the critical flux further (from the isotropic value). The flux for anisotropic self-similarly evolving crystals may even be negative which implies the existence of self-similar melting crystals. Self-similar melting does not occur under isotropic surface tension (in the absence of interface kinetics). In a subsequent work, we consider the stability of the self-similar shapes [20].

This paper is organized as follows: in Section 2, we present the governing equations and review the linear stability analysis. We formulate the nonlinear self-similar theory in Section 3. In Section 4, we present the numerical scheme. We present numerical results and comparisons to linear theory in Section 5. Conclusions and a discussion of work in progress are given in the last section.

2. Governing equations and linear stability analysis

2.1. Governing equations

We consider a two-dimensional solid crystal growing quasi-statically in a supercooled liquid phase. The interface Σ separates the solid phase Ω_1 from the liquid phase Ω_2 (Fig. 1). We assume for simplicity that local equilibrium holds at the interface, and the thermal diffusivities of the two phases are identical. The results presented herein apply more generally however [21]. Using the nondimensionalization given in Refs. [1,2], the following equations govern the growth of the crystal:

$$\nabla^2 T_i = 0 \quad \text{in } \Omega_i \quad i = 1, 2, \tag{1}$$

$$V = (\nabla T_1 - \nabla T_2) \cdot \mathbf{n} \quad \text{on } \Sigma, \tag{2}$$

$$T_1 = T_2 = -\tau(\mathbf{n})\kappa \quad \text{on } \Sigma, \tag{3}$$

$$J = \frac{1}{2\pi} \int_{\Sigma} V \, \mathrm{d}s, \tag{4}$$

and the interface Σ evolves via

$$\mathbf{n} \cdot \frac{\mathrm{d}\mathbf{x}}{\mathrm{d}t} = V \quad \text{on } \Sigma, \tag{5}$$

where T_i is the temperature field, $i = 1$ for solid phase and $i = 2$ for liquid phase, V is the normal velocity of the interface, $\mathbf{n}$ is the unit normal directed towards Ω_2, κ is the curvature, τ is the anisotropic surface tension and J is the far-field heat flux. In Eq. (4) we have used the fact that the

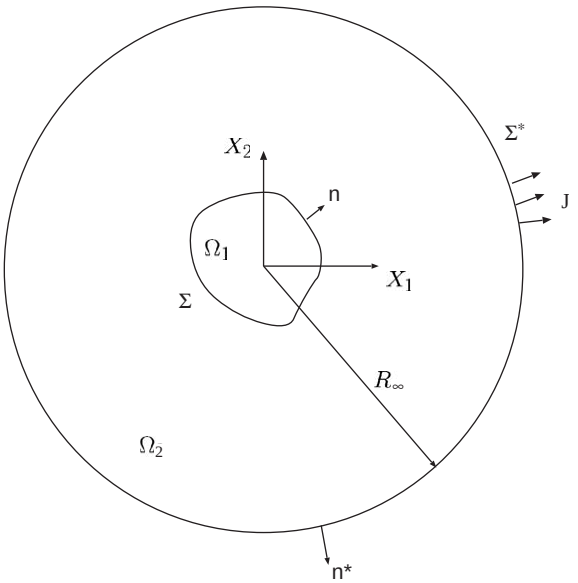

Fig. 1. A schematic diagram of a perturbed circular crystal in liquid.

T_i are harmonic [2] so that J specifies the time derivative of the area of the solid phase. In 2D, the normal vector $\mathbf{n} = (n_1, n_2)$ can be characterized in terms of a single variable which can be taken to be the tangent angle $\theta = \tan^{-1}(-n_1/n_2)$, i.e. the angle the tangent vector makes with the x_1-axis. Thus the anisotropic surface tension $\tau = \tau(\theta)$. Further, $\tau(\theta) = \gamma(\theta) + \gamma''(\theta)$ where $\gamma(\theta)$ is the anisotropic surface energy. For a general m-fold anisotropy,

$$\gamma(\theta) = 1 + v_m \cos m\theta,$$

and

$$\tau(\theta) = 1 - \left(m^2 - 1\right) v_m \cos m\theta, \tag{6}$$

where v_m is the strength of the anisotropy (e.g. see Ref. [22]).

2.2. Linear analysis

In this section, we analyze the linear stability of a growing crystal following [13,14,23,2]. We take the perturbed crystal-melt interface to be given by a linear combination of Fourier modes,

$$r(\theta, t) = R(t) + \sum_{k=2}^{\infty} \delta_k(t) \cos k\theta, \tag{7}$$

where $R(t)$ is the radius of a underlying growing circle. We assume that the anisotropy v_m is on the same order as δ_k so that products of v_m and δ_k are neglected. We obtain the rate of area growth

$$R(t)\frac{\mathrm{d}R}{\mathrm{d}t} = J(t), \tag{8}$$

and the growth rate of the k-th mode perturbation,

$$\left(\frac{\delta_k}{R}\right)^{-1} \frac{\mathrm{d}}{\mathrm{d}t}\left(\frac{\delta_k}{R}\right) = \frac{(k-2)(J - J_k)}{R^2}, \tag{9}$$

where the critical flux and the linear flux constant are

$$J_k(t) = \frac{C_k}{R(t)},$$
$$C_k = \frac{2k(k^2-1)}{k-2} \cdot \begin{cases} 1 - v_m R/\delta_m & k = m, \\ 1 & k \neq m. \end{cases} \tag{10}$$

The far-field temperature is

$$T_\infty(t) = -J \log\left(\frac{R_\infty}{R}\right) - 1/R. \tag{11}$$

Eq. (9) shows that perturbations grow (decay) for $J > J_k$ ($J < J_k$). Since $J_k \sim 1/R$, taking a constant flux $J > 0$ results in the instability of perturbations with successively higher wavenumbers as the crystal grows. This is the Mullins–Sekerka instability [13].

When $J = J_k$, the perturbation is unchanged in time and so linear theory predicts self-similar growth if the crystal contains a single mode k. That is, the shape factor $\alpha = \delta_k(t)/R(t)$ is time-independent. Note that when $k = m$, the critical flux J_m is a decreasing function of the anisotropy ratio v_m/α. In fact, for $v_m/\alpha > 1$, the critical flux $J_m < 0$. This predicts the existence of linear self-similar melting shapes. Such shapes do not exist for isotropic surface tension $v_m = 0$. As we see later, self-similar melting shapes for the full nonlinear problem do indeed exist for the anisotropic case.

When $k = 2$, Eq. (10) shows that when $v_m = 0$, $C_k \to \infty$ and self-similar evolution is not possible (perturbations always decay) [13]. In contrast, when $v_2 \neq 0$, it may be possible to achieve self-similar evolution since the ratio $(1 - v_m/\alpha)/(k-2)$ may be finite. However, the problem is indeterminate (since any finite flux J can be used). Later, a nonlinear investigation of this case will be performed which suggests that nonlinear 2-fold dominated self-similar shapes exist when $v_2 > 0$.

Eqs. (8)–(11) are qualitatively similar to those obtained by Cristini and Lowengrub [2] for the isotropic case ($v_m = 0$) in 3D. In 3D, the isotropic critical flux is [2]

$$J_k^{3D}(t) = \frac{(k+2)(k-1)(1+2k)}{k-2}, \tag{12}$$

where k is the polar wavenumber of a spherical harmonic perturbation. As discussed in Ref. [2], the critical flux in 3D is independent of R, which implies that the Mullins–Sekerka instability in 3D can be suppressed by taking a constant far-field flux $J > 0$ since no new unstable modes are created during the evolution (in the absence of interface kinetics). In contrast, Eq. (9) shows that in 2D, Mullins–Sekerka instability can be suppressed if the 2D far-field flux decreases as $J \sim 1/R$. This difference exactly reflects the different scaling of the flux between 2D and 3D (area vs. volume

evolution). If one rescales the far-field flux J by R, i.e. $\tilde{J} = RJ$, then $R^2 \mathrm{d}R/\mathrm{d}t = \tilde{J}$ and the right-hand side of Eq. (9) becomes $(k-2)(\tilde{J} - C_k)/R^3$. These equations are identical to those obtained in 3D if C_k is replaced by J_k^{3D} and the 3D far-field flux is $\tilde{J}$ [2]. This suggests that our 2D work provides insight to the 3D problem.

3. Nonlinear self-Similar theory

In this section, we derive the full nonlinear system of equations that a self-similar evolving crystal must satisfy. We begin by re-formulating Eqs. (1), (2) and (3) as a system of boundary integral equations where we represent the temperature field through a single-layer potential. This yields the first-kind Fredholm integral equations [28,29]

$$-\tau(\theta)\kappa(\mathbf{x}) = \int_{\Sigma} G(\mathbf{x}-\mathbf{x}')V(\mathbf{X}')\,\mathrm{d}s(\mathbf{x}') + T_\infty, \quad (13)$$

$$J = \frac{1}{2\pi}\int_{\Sigma} V(\mathbf{x}')\,\mathrm{d}s(\mathbf{x}'), \quad (14)$$

where $G(\mathbf{x}) = 1/2\pi\log|\mathbf{x}|$ is the Green's function, $V(\mathbf{x})$ is the normal velocity of the interface Σ, and $T_\infty(t)$ is the far-field temperature.

A fundamental feature of self-similar evolution is that time and space are separable. Therefore, the position vector of the interface during self-similar evolution can be written as

$$\mathbf{x} = R(t)\tilde{\mathbf{x}}(s), \quad (15)$$

where $\tilde{\mathbf{x}}(s)$ specifies the self-similar shape, $R(t)$ is a scaling function related to the effective radius of the growing crystal, and s is the arclength along the self-similar interface. Substituting Eq. (15) into Eq. (13), we obtain

$$-\tau\big(\tilde{\theta}(s)\big)\tilde{\kappa}(s) = JR\frac{\pi}{\tilde{A}}\int_{\tilde{\Sigma}} \tilde{\mathbf{x}}(s')\cdot\mathbf{n}(s')G\big(\tilde{\mathbf{x}}(s) - \tilde{\mathbf{x}}(s')\big)\,\mathrm{d}s' + \tilde{T}_\infty(t), \quad (16)$$

where $\tilde{\theta}$ is the tangent angle of the self-similar shape, $\kappa = \tilde{\kappa}/R$ and we have used, from Eq. (14), that $J = \tilde{A}/\pi R\dot{R}$, $\dot{R} = \mathrm{d}R/\mathrm{d}t$, and $\tilde{T}_\infty(t) = 1/\pi, \tilde{A}\dot{R}R^2\log R + T_\infty R$, where $\tilde{A}$ is the area of the self-similar shape $\tilde{\mathbf{x}}$.

To proceed further, we separate time and space by differentiating Eq. (16) with respect to arclength. This gives

$$-\big(\tau(\tilde{\theta})\tilde{\kappa}\big)_s / G[\tilde{\mathbf{x}}]_s = JR\frac{\pi}{\tilde{A}} = C, \quad (17)$$

where the notation $(.)_s = \partial/\partial s$, C is the heat flux constant (in space and time), and

$$G[\tilde{\mathbf{x}}](s) = \int_{\tilde{\Sigma}} \tilde{\mathbf{x}}'\cdot\mathbf{n}(\tilde{s}')G\big(\tilde{\mathbf{x}}(s) - \tilde{\mathbf{x}}(s')\big)\,\mathrm{d}s'. \quad (18)$$

We note from Eq. (17) that the coefficient of the integral term in Eq. (16) is constant in time. The resulting equation is identical to the 3D equation for nonlinear self-similar crystal shapes if the constant C is replaced by the 3D nonlinear self-similar flux, G is replaced by the 3D Green's function and $\tilde{T}_\infty(t)$ is defined appropriately [21]. This further supports our contention that 2D analysis can provide insight to 3D self-similar evolution.

The spatial part of Eq. (17) gives

$$-G_s = \frac{1}{C}\big(\tau(\tilde{\theta})\tilde{\kappa}\big)_s, \quad (19)$$

which is a nonlinear, nonlocal eigenvalue problem where the shape is the eigenvector and the inverse heat flux constant is the eigenvalue. To remove the constant C, we differentiate Eq. (19) to get

$$\big(\tau(\tilde{\theta})\tilde{\kappa}\big)_{ss}G_s - G_{ss}\big(\tau(\tilde{\theta})\tilde{\kappa}\big)_s = 0. \quad (20)$$

All self-similar shapes must satisfy this equation. Since circles automatically satisfy this equation in the isotropic case ($\tau = 1$), Eq. (20) must have nonunique solutions in the isotropic case if noncircular self-similar shapes exist. It is also reasonable to expect that nonunique solutions may exist in the anisotropic case as well. However, Eq. (20) involves fourth order derivatives of the interface position and is highly nonlinear and nonlocal. Hence, even if solutions exist, they may be difficult to obtain. In the appendix, we develop a quasi-Newton method to solve Eq. (20) numerically and demonstrate numerically that noncircular solutions to Eq. (20) do exist for both the isotropic and anisotropic cases.

If we can solve Eq. (20) for the shapes, we can determine the constant C through Eq. (19) and obtain the corresponding far-field flux $J(t) =$

$\tilde{A}C/\pi R(t)$. The original dimensionless far-field temperature T_∞ is given by

$$T_\infty(t) = \frac{\tilde{T}_\infty(t)}{R} - J(t)\log(R), \tag{21}$$

where $\tilde{T}_\infty$ is determined through Eq. (16) if we know $\tilde{\mathbf{x}}(s)$ and the flux J. Notice that if one rescales J by R, then rescaled flux $\tilde{J} = RJ = \tilde{A}C/\pi$ is constant. Once the flux constant C is known, the scaling function $R(t)$ is given by

$$R(t) = (1 + 3Ct)^{1/3}. \tag{22}$$

This is exactly the same growth law for self-similar shapes as that obtained by Cristini and Lowengrub in 3D (with C replaced by the 3D flux), even though the fluxes scale differently in 2D and 3D. This suggests that the underlying mechanism for self-similar evolution is the same in 2D and 3D.

4. Self-Similar shapes

4.1. Isotropic surface tension

In this section, we implement the quasi-Newton scheme to solve Eq. (20) when $\tau = 1$. We begin by considering a 4-fold dominant self-similar shape. We use as an initial guess a perturbed sphere with wavenumber $k = 4$ (i.e. we prescribe $\tilde{\delta}_4$ and set the amplitudes of other modes to zero except for $\tilde{\delta}_0$ which is set to 1). After the self-similar shape is found, the nonlinear flux constant is obtained from Eq. (17). In this calculation, we set the number of mesh points to be $N = 256$ along the interface. We find numerically that a solution to Eq. (20) exists and that the Newton solver yields up to 10^{-6} precision when solving Eq. (20). For all mesh points, at least 5 digits after the decimal point are identical for the ratio on the left hand side of Eq. (17). Fig. 2(a) shows the difference of flux constants between the linear theory and nonlinear simulations versus the square of the shape factor for the 4-fold dominant nonlinear self-similar shape. The shape factor is

$$\delta/R = \max|\tilde{\mathbf{x}}|/\tilde{R}_{\text{eff}} - 1|, \tag{23}$$

where $\tilde{\mathbf{x}}$ is the position vector from the centroid of the shape to the interface and $\tilde{R}_{\text{eff}}$ is the effective

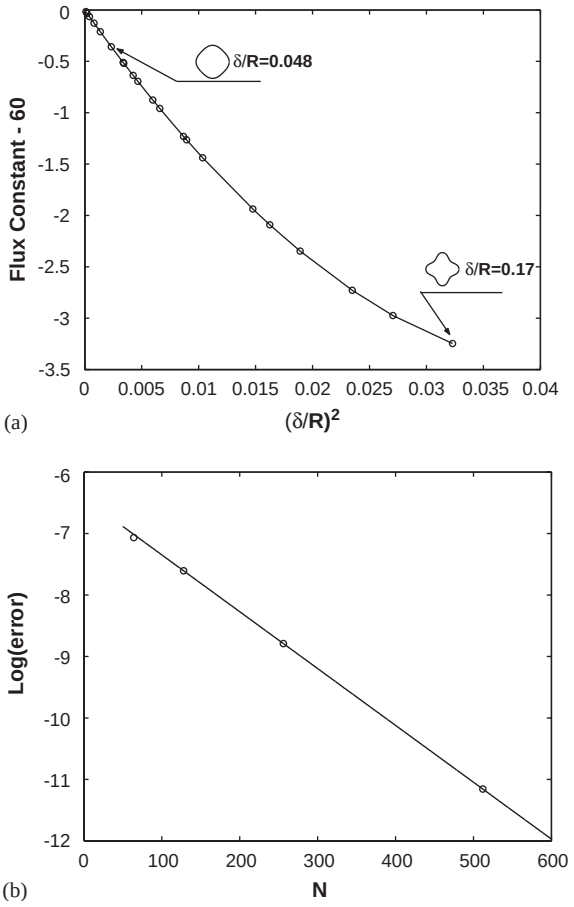

Fig. 2. (a) The difference of flux constant between linear prediction and nonlinear theory for a 4-fold dominant self-similar shape. The nonlinear flux constants are calculated through Eq. (17), the linear flux constant is 60 by Eq. (10) with $k = 4$. (b) Resolution study of a 4-fold dominant self-similar shape.

radius of the nonlinear (self-similar) shape. The different nonlinear solutions are obtained by varying $\tilde{\delta}_4$ for the initial guess. Two associated interface morphologies are shown corresponding to small and large values of δ/R, respectively We note that, according to linear theory, the flux constant is related to the wavenumber k only (i.e independent of δ/R) and is equal to 60 (from Eq. (10)) for a $k = 4$ self-similar shape. As we can see, when δ/R is small, the deviation of the nonlinear results from linear theory is quadratic in δ/R, as expected. However, when δ/R is large, the deviation is no longer quadratic. Nonlinear

effects result in a lowered flux constant. Interestingly, the Fourier series descriptions of these nonlinear self-similar shapes involve only mode 4 and its harmonics (integer multiples of wavenumber 4). Analogous results were found to hold for other k-fold self-similar shapes as well.

To assess the accuracy of the quasi-Newton solver, we perform a resolution study of a 4-fold dominant self-similar shape. The results for isotropic surface tension are shown in Fig. 2(b), where the error is measured in terms of the magnitude of δ/R. Analogous results hold when the surface tension is anisotropic. To determine the error, the self-similar shapes are computed using four resolutions, $N = 64$, 128, 256, 512 with the initial guess $\tilde{\delta}_4 = 0.07$. The quasi-Newton solver is found to be spectrally accurate with the following error expansion

$$\left(\frac{\delta}{R}\right)_N = \left(\frac{\delta}{R}\right)^* + \beta_1 e^{-\beta_2 N}, \tag{24}$$

where $(\delta/R)^*$ is the exact solution. Taking $(\delta/R)_N$ from the results of our numerical simulations ($(\delta/R)_N = 7.005 \times 10^{-2}$, 6.9699×10^{-2}, 6.9354×10^{-2}, 6.9216×10^{-2}, for $N = 64$, 128, 256, 512, respectively), we obtain $\beta_1 = 0.0016239$, $\beta_2 = 0.0092455$, and the exact solution $(\delta/R)^* = 0.0692017$. The error is equal to the difference between $(\delta/R)_N$ and $(\delta/R)^*$.

We next consider the effects introduced by different symmetries. Fig. 3 shows the flux constants and morphologies for general k-fold self-similar crystals. We start the calculation by specifying $\tilde{\delta}_k$ as the initial guess. We plot the linear theory prediction as the solid curve $C = 2k(k^2 - 1)/(k - 2)$ from Eq. (10). Symbols denote the nonlinear simulation results. The flux constants are in very good agreement with linear theory when the perturbations are small. For self-similar shapes with large δ/R, the flux constants are smaller than the prediction of linear theory. The scaling with k is similar to but slightly smaller than the linear theory as can be seen from the dashed curve, which shows a fit of nonlinear data $C = 3k(k^{1.7} - 1)/(k - 2)$. Observe that the nonlinear self-similar shapes with small δ/R are convex while those with large δ/R have concave regions (negative curvature).

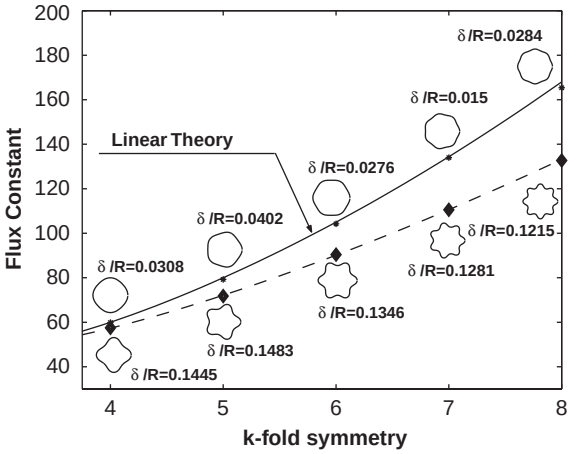

Fig. 3. Flux constants of self-similar shapes and selected morphologies with isotropic surface tension. Flux constants from linear theory (solid line) are given by Eq. (10), $C = 2k(k^2 - 1)/(k - 2)$. Symbols denote the nonlinear quasi-Newton results. The dashed line is a best fit for the nonlinear self-similar shapes with large shape factor δ/R, $C = 3k(k^{1.7} - 1)/(k - 2)$.

As an additional confirmation of self-similarity as well as a test of robustness, these self-similar shapes (and also those presented in the next section) were used as initial data in a nonlinear time evolution code [20]. In all cases, the resulting evolution was self-similar up to small numerical errors.

Finally, we note that when the surface tension is isotropic, there are no self-similar solutions with negative critical flux (i.e. melting).

4.2. Anisotropic surface tension

We next consider the effect of anisotropic surface tension. Fig. 4 shows the flux constants and morphologies for general m-fold self-similar crystals with a number of different anisotropies v_m. The flux constants are divided by the linear isotropic flux constant $C = 2k(k^2 - 1)/(k - 2)$ and are shown as a function of the anisotropy ratio v_m/α (recall $\alpha = \delta/R$). Symbols denote the nonlinear quasi-Newton results and the solid line is the result of linear theory. The dotted straight lines on the (left) y-axis marked by $k = 4$, 6 and 8 correspond to isotropic results from Fig. 3.

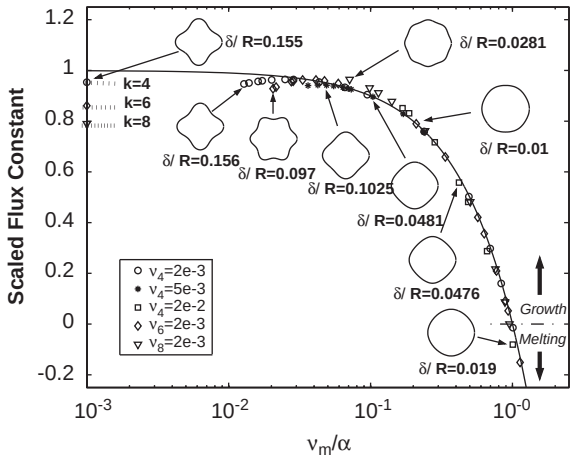

Fig. 4. Flux constants of self-similar shapes and selected morphologies with anisotropic surface tension. The flux constants are divided by the linear isotropic flux constant $C = 2k(k^2-1)/(k-2)$ and are shown as a function of the anisotropy ratio v_m/α (recall $\alpha = \delta/R$). Symbols denote the nonlinear quasi-Newton results and the solid line is the result of linear theory. The dotted horizontal lines on the left y-axis correspond to isotropic results. The dot-dashed horizontal line on the right y-axis denotes the value $C = 0$ below which melting occurs.

The numerical results strongly suggest that nonlinear self-similar shapes exist. When the anisotropy v_m and the shape factor α are both small, the results agree well with the prediction of linear theory (linear theory assumes that v_m and α are of the same order).

The horizontal dashed-dot line at the (right) y-axis in Fig. 4 marks the zero flux value (equilibrium shape). Below this value, the flux is negative and the solutions correspond to melting. Note that for $v_m/\alpha > 1$, the nonlinear simulations generate negative flux constants. This implies the existence of nonlinear self-similar shapes during melting in the presence of anisotropy.

When $v_m/\alpha \to 0$, either v_m tends to 0 (isotropic limit) with α finite or α is large and v_m is finite. In both cases, this limit corresponds to the nonlinear regime and deviation from the linear prediction is seen. The scaled flux constants are smaller than the linear prediction and are decreasing functions of m and v_m. Moreover, the nonlinear results do not just depend on the ratio v_m/α. A careful examination of the results indicates that the flux constants also weakly depend on v_m and α individually.

Fig. 4 also suggests that there are many ways to achieve a desired crystal shape. For example, consider a 4-fold shape with $\delta/R \approx 0.048$. Our results indicate that this shape can be obtained either by using $v_4 = 2 \times 10^{-3}$ with flux constant $C_4 = 56.8$ or by using $v_4 = 2 \times 10^{-2}$ with a smaller flux constant $C_4 = 33.5$. Moreover, the same shape can achieved with $v_4 = 0$ (isotropic) with an even larger flux. See, for example, the 4-fold shapes with $\delta/R \approx 0.156$.

Next we investigate the case when $m = 2$. Recall from Section 2.2 this case is indeterminate and self-similar solutions do not exist for the isotropic case. We found numerically that there exist solutions to Eq. (20) when $v_2 > 0$ (the solutions actually contain all even modes). All solutions we have found thus far have associated critical fluxes $J_2 > 0$ and so describe growing crystals. One such nonlinear self-similar shape is plotted in Fig. 5. In this case, $v_2 = 0.15$ and the flux $J_2 = 99.81$. Interestingly, this case yields the value $v_2/\alpha = 1.39$ which, when plugged into Eq. (10), predicts a linear critical flux of negative infinity.

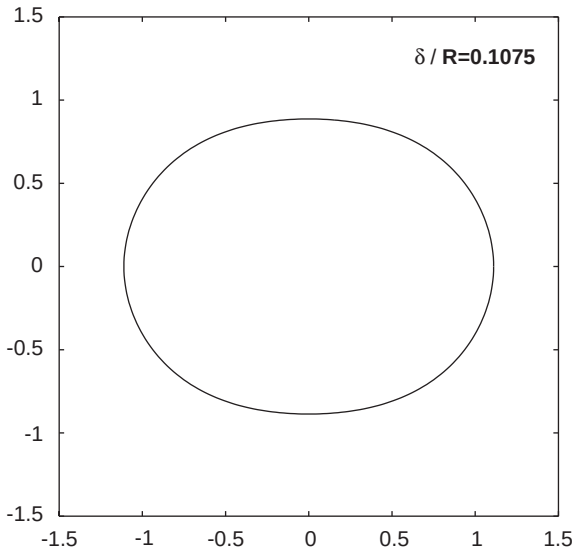

Fig. 5. A 2-fold self-similar shape with $v_2 = 0.15$ and flux $J_2 = 99.81$ (growth). Note that the isotropic linear flux is $+\infty$ which is why this plot is not included in Fig. 4.

5. Conclusions and future work

In this paper, we developed a nonlinear theory of self-similar crystal growth in 2D. Our analysis reveals that the governing equations for nonlinear self-similar crystals are qualitatively similar in 2D and 3D once the difference between the 2D and 3D heat fluxes (i.e. area vs. volume growth) is scaled out. Thus, our work here provides insight to the 3D problem.

Our numerical results indicate that nonlinear, noncircular self-similarly evolving crystals do indeed exist. Our results also suggest that for a k-fold dominant self-similar shape, only mode k and its harmonics (integer multiples of the wavenumber k) appear in the Fourier series description of the interface. In the isotropic case, k is arbitrary and only growing solutions exist. When the surface tension is anisotropic, k is determined by the form of the anisotropy and both growing and melting solutions exist.

One of the effects of nonlinearity is to reduce the nonlinear critical flux compared to that predicted by linear theory. One of the effects of anisotropy is to reduce the critical flux further (from the isotropic value) and the flux may even be negative. When the flux for anisotropic self-similarly evolving crystals is negative, self-similar melting occurs. Further, we have demonstrated the existence of nonlinear self-similar growing crystals with 2-fold anisotropy.

In a companion paper [20], we will discuss the stability of the self-similar shapes found here and the implications for controlling the shape of growing and melting crystals. Using a new spectrally accurate boundary integral method with a time and space rescaling that enables accurate long-time simulations to be performed, our preliminary results reveal that the self-similar shapes are stable to perturbations of the critical flux and are unstable to low-mode perturbations of the shape which may either be present initially or may be produced by nonlinear interactions. However, when the dominant wavenumber of the self-similar shape is small, the instability takes a long time to develop. Thus, this leads to the possibility of controlling crystal shapes using the critical flux. When the instability fully develops, the growth shape will be dominated by the fastest growing mode as first suggested by Cristini and Lowengrub [1]. As an alternative means to controlling the shape, this can be exploited [1,2] to produce compact growing crystals with desired symmetries by taking a heat flux such that a particular mode has the fastest growth rate.

The analysis described in this paper (and above) is based on the idea that the heat flux can be controlled at infinity. Clearly, this is an idealization. When the domain is finite, we expect that our analysis holds when the volume fraction of crystals is low and the crystals are located far from the domain boundary. When crystal/crystal and crystal/boundary interactions are important, the analysis must be modified to account for the fact that the local flux applied to each crystal differs from the far-field flux. Work needs to be done to determine whether crystal shapes can be controlled in a precise manner in this context. Nevertheless, we anticipate that the Mullins–Sekerka instability can still be suppressed to obtain compact crystal shapes by varying the far-field temperature as described here, even when crystal/crystal and crystal/boundary interactions are important.

Acknowledgements

The authors thank the generous computing resources from the Minnesota Supercomputer Institute, the Network and Academic Computing Services at University of California at Irvine (NACS), and the hospitality of Institute for Mathematics and its Application. S. Li thanks the generosity of the Department of Biomedical Engineering at UCI. S. Li also thanks Yubao Zhen for technical discussions. J. Lowengrub and V. Cristini thank the National Science Foundation (division of mathematics) for partial support.

Appendix A. Quasi-Newton scheme for self-similar shapes

In this appendix, we present a quasi-Newton method to solve Eq. (20) to obtain the self-similar shape of a growing crystal. Rather than using the

arclength parameterization, we find it more convenient to parameterize the interface by the polar angle α and solve for the Fourier modes in the polar angle representation. In order to begin our computation we first specify the radius of interface to be a combination of *cosine* Fourier modes:

$$\tilde{r}(\alpha) = \sum_{k=0}^{N-1} \tilde{\delta}_k \cos k\alpha, \tag{A.1}$$

where N is the total number of modes and $\tilde{\delta}_k$ is the coefficient of the kth mode. Then the interface positions $(\tilde{x}, \tilde{y})$ are given as

$$\begin{aligned} \tilde{x}(\alpha) &= \tilde{r}(\alpha)\cos\ \alpha \\ \tilde{y}(\alpha) &= \tilde{r}(\alpha)\sin\ \alpha. \end{aligned} \tag{A.2}$$

We note that the arclength variable s in Eq. (20) is related to α via $s_\alpha = \sqrt{\tilde{x}_\alpha^2 + \tilde{y}_\alpha^2}$.

Let $\mathbf{f}$ be a discretization of the left-hand side of Eq. (20) where $\tilde{\kappa}$, $\mathbf{n}$ are approximated with spectral accuracy using pseudo-spectral methods and the integral $G[\tilde{\mathbf{x}}]$ is approximated with spectral accuracy. The quadrature of the integral is nontrivial because of the logarithmic singularity of the 2D Green's function. The tangent angle θ can be recovered from the curvature by integrating the relation $\tilde{\theta}_\alpha = s_\alpha \tilde{\kappa}$. See Refs. [26,25] for details.

The discrete problem consists of finding $\tilde{\delta}$'s for which

$$\mathbf{f}(\tilde{\delta}_0, \tilde{\delta}_1, \tilde{\delta}_2, \ ..., \ \tilde{\delta}_N) = 0, \tag{A.3}$$

at the interface node points $\alpha_i = i\Delta\alpha$ with $\Delta\alpha = 2\pi/N$ for $i = 0, \ldots, N-1$. We use the classical quasi-Newton method, together with a line-search method [24] to solve Eq. (27). This algorithm is similar in spirit to that used by Thompson and Voorhees to determine equilibrium shapes of particles in elastically stressed coherent solids [27].

The quasi-Newton method uses the iteration

$$\tilde{\boldsymbol{\delta}}^{j+1} = \tilde{\boldsymbol{\delta}}^{j} - \mathbf{J}^{-1}\mathbf{f}(\tilde{\boldsymbol{\delta}}^{j}), \qquad \mathrm{j} = 0, 1, 2, \ ..., \tag{A.4}$$

where $\mathbf{J}$ is the Jacobian matrix, $\mathbf{J} = \nabla_{\tilde{\delta}}\mathbf{f}$. However, it is very difficult to determine $\mathbf{J}$ explicitly for our problem since $\mathbf{f}$ is highly nonlinear and nonlocal and thus depends on the $\tilde{\delta}_1, \tilde{\delta}_2 \ldots$ in a very complicated way. Therefore, we use a finite difference approximation to calculate the matrix $\mathbf{J}$,

$$J_{ij} \approx \frac{f_i(\tilde{\delta}_0, \tilde{\delta}_1, \tilde{\delta}_2, \ ..., \ \tilde{\delta}_j + h, \ ..., \ \tilde{\delta}_N) - f_i(\tilde{\delta}_0, \tilde{\delta}_1, \tilde{\delta}_2, \ ..., \ \tilde{\delta}_j, \ ..., \ \tilde{\delta}_N)}{h}, \tag{A.5}$$

where h is small. In practice, we find that the iteration scheme is robust but takes longer to converge when the anisotropy, initial shape perturbation or wavenumber is large. The optimal choice of h seems to depend on the initial guess and typically we take $10^{-8} \leqslant h \leqslant 10^{-5}$ where h is chosen empirically to achieve the most rapid convergence and the smallest value of $\max|\mathbf{f}|$. The quasi-Newton iteration is performed until $\max|\mathbf{f}|$ is less than a prescribed tolerance. Convergence of the iteration to different self-similar shapes is achieved by varying the initial guess.

References

[1] V. Cristini, J. Lowengrub, Three-dimensional crystal growth. II: nonlinear simulation and control of the Mullins–Sekerka instability, J. Crystal Growth, 2003 in press.

[2] V. Cristini, J. Lowengrub, Three-dimensional crystal growth. I: linear analysis and self-similar evolution, J. Crystal Growth 240 (2002) 267.

[3] J.S. Langer, Instability and pattern formation in crystal growth, Rev. of Mod. Phys. 52 (1980) 1.

[4] G.B. McFadden, S.R. Coriell, R.F. Sekerka, Effect of surface free energy anisotropy on dendrite tip shape, Acta Mater. 48 (2000) 3177.

[5] G.B. McFadden, S.R. Coriell, R.F. Sekerka, Analytic solution for a non-axisymmetric isothermal dendrite, J. Crystal Growth 208 (2000) 726.

[6] D.A. Kessler, H. Levine, Pattern selection in three dimensional dendritic growth, Acta Metall. 36 (1988) 2693.

[7] T. Uehara, R.F. Sekerka, Phase field simulations of faceted growth for strong anisotropy of kinetic coefficient, J. Crystal Growth 254 (2003) 251.

[8] M.E. Glicksman, A. Lupulescu, M.B. Koss, Melting in Microgravity, J. Thermophys. Heat Transfer. 17 (1) (2003) 69.

[9] G. Wulff, Z. Kristallogr. Mineral. 34 (1901) 449.

[10] D.M. Anderson, G.B. McFadden, A.A. Wheeler, A phase-field model with convection: sharp interface asymptotics, Physica D 151 (2001) 305.

[11] A. Pimpinelli, J. Villain, Physics of Crystal Growth, Cambridge University Press, Cambridge, 1998.

[12] B.K. Johnson, R.F. Sekerka, R. Almgren, Thermodynamic basis for a variational model for crystal growth, Phys. Rev. E 60 (1999) 705.

[13] W.W. Mullins, R.F. Sekerka, Morphological stability of a particle growing by diffusion or heat flow, J. Appl. Phys. 34 (2) (1963) 323.
[14] S.R. Coriell, R.L. Parker, Stability of the shape of a solid cylinder growing in a diffusion field, J. Phys. 36 (1965) 632.
[15] S.C. Hardy, S.R. Coriell, Morphological stability of cylindrical ice crystals, J. Crystal Growth 5 (1969) 329.
[16] S.C. Hardy, S.R. Coriell, Morphological stability of a cylinder, J. Res. Bureau of Standards–A. Phys. Chem. 73A (1) (1969) 65.
[17] K.G. Libbrecht, Morphogenesis on ice : the physics of snow crystals, Eng. Sci. 1 (2001) 10.
[18] S.R. Coriell, R.L. Parker, in: H.S. Peiser (Ed.), Crystal Growth, Pergamon, Oxford, 1967, p.703.
[19] L.N. Brush, R.F. Sekerka, A numerical study of two-dimensional crystal growth forms in the presence of anisotropic growth kinetics, J. Crystal Growth 96 (1989) 419.
[20] S. Li, P. Leo, J. Lowengrub, V. Cristini, Morphological control of crystal growth, in preparation.
[21] S. Li, Morphological control of crystal growth, Ph.D. 2005 expected, University of Minnesota.
[22] Y. Saito, Statistical Physics of Crystal Growth, World Scientific, Singapore, 1996.
[23] S.R. Coriell, R.F. Sekerka, The effect of the anisotropy of surface tension and interface kinetics on morphological stability, J. Crystal Growth 34 (1976) 157.
[24] W.H. Press, B.P. Flannery, S.A. Teukolsky, W. Vetterling, Numerical Recipes in Fortran, 2nd Edition, Cambridge University Press, Cambridge, January 15, 1992.
[25] T.Y. Hou, J.S. Lowengrub, M.J. Shelley, Boundary integral methods for multicomponent fluids and multi-phase aterials, Comput. Phys. 169 (2) (2001) 302.
[26] H.J. Jou, P. Leo, J. Lowengrub, Microstructural evolution in inhomogeneous elastic media, J. Comput. Phys. 131 (1997) 109.
[27] M.E. Thompson, P.W. Voorhees, Equilibrium particle morphologies in elastically stressed coherent solids, Acta Mater. 47 (3) (1999) 983.
[28] J.Y. Zhu, X.F. Chen, T.Y. Hou, An efficient boundary integral method for the Mullins-Sekerka problem, J. Comput. Phys. 127 (1996) 246.
[29] S.G. Mikhlin, Integral Equations and their Applications to certain Problems in mechanics, Mathematical Physics and Technology, Pergamon, New York 1957.